Advanced Powder Technology

Aging effects on airflow distribution and micron-particle transport and deposition in a human lung using CFD-DPM approach

--Manuscript Draft--

Manuscript Number:	ADVPT-D-21-00705R1
Article Type:	Original Research Paper
Keywords:	Aging effect, Airflow, Aerosol particle transport and deposition (TD), Lung, Inhalation, Drug delivery, Cutting method
Corresponding Author:	Ming Zhao AUSTRALIA
First Author:	Mizanur Rahman, Rahman
Order of Authors:	Mizanur Rahman, Rahman
	Ming Zhao
	Mohammad S Islam
	Kejun Dong
	Suvash C saha
Abstract:	Understanding the transportation and deposition (TD) of inhaled aerosol particles in human lung airways is important for health risk assessment and therapeutic efficiency of targeted drug delivery. The particle TD into a human lung depends on lung anatomy, breathing pattern, as well as particle properties. The breathing capacity and lung airway diameters can be reduced by about 10% every 10 years after the age of 50. However, the age-specific particle TD in human lungs, particularly in the aged, has not been well understood in literature. This study investigates the particle TD in the lungs of people aged 50-70 years, using computational fluid dynamics (CFD). A new cutting method that splits the lung model into different sections has been developed as a feasible CFD method to simulate the particle TD in G0 to G14 lung airways. The inhalation of micron scale particles with three diameters (5 μm, 10 μm and 20 μm) and a constant air flow rate in inhalation is considered. It is found that different sized particles are deposited in different generation airways. Nearly 100% of 20 μm particles are deposited in the upper lung airways (G0-G5) and no particles pass through G7. Particles can go into deeper airways as their diameter decreases. When the particle size is decreased to 5 μm, over 48% of particles can pass through G14 and enter the deeper lung airways. An increase in age causes more particles to deposit in the upper airway and fewer particles to enter the deeper airways.

Graphic al

Click here to

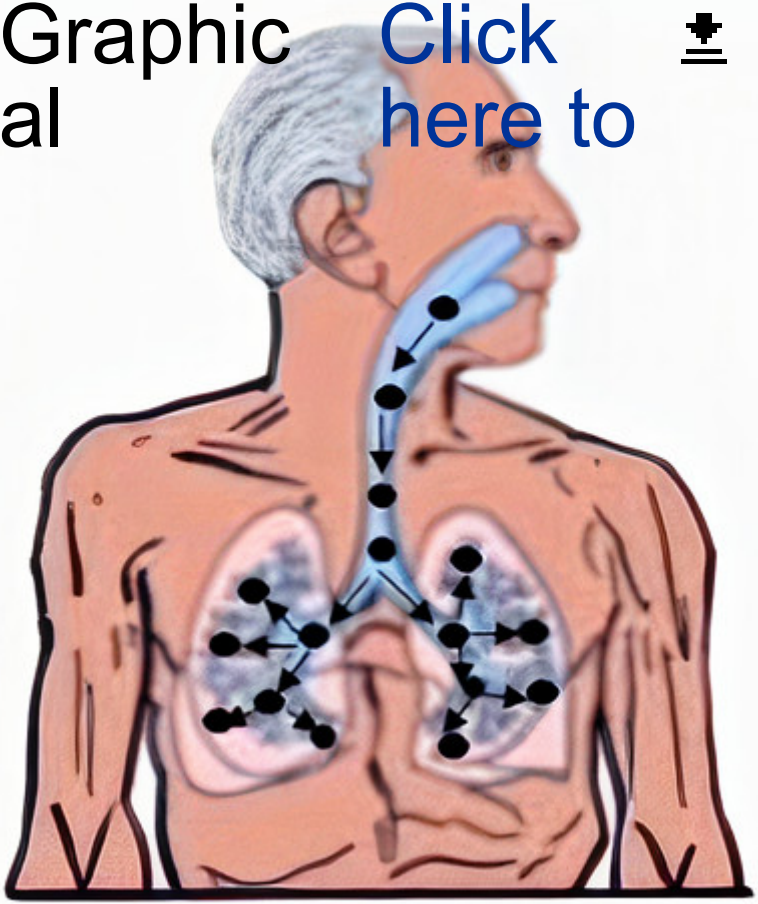

- Particle transportation and deposition (TD) in human lungs of people aged 50-70 simulated.
- A new cutting method developed to simulate particle TD in G0 to G14 lung airways.
- 20 μm particles are mostly deposited in G0-G5 but do not pass through G7.
- Over 48% of 5 μm particles can pass through G14 and enter the deeper lung airways.
- Escaping rate in each generation decreases with the increase of age.
- The total deposition efficiency increases with the increase of age.

Aging effects on airflow distribution and micron-particle transport and deposition in a human lung using CFD-DPM approach

Md. M Rahman [1, 2], Ming Zhao [1, *], Mohammad S Islam [3], Kejun Dong[4], and Suvash C Saha [3]

[1] School of Computing, Engineering, and Mathematics, Western Sydney University, Penrith, NSW, 2751, Australia ; 19615253@student.westernsydney.edu.au

[2]Department of Mathematics, Faculty of Science, Islamic University, Kushtia-7300, Bangladesh

[3]School of Mechanical and Mechatronic Engineering, University of Technology Sydney, Ultimo, NSW 2007, Australia ; mohammadsaidul.islam@uts.edu.au (M.S. I); suvash.saha@uts.edu.au (S.C.S);

[4] Center for Infrastructure Engineering, Western Sydney University, 2751 Penrith, NSW, Australia; kejun.dong@westernsydney.edu.au

***Correspondence: M.Zhao@westernsydney.edu.au ; Tel.: + 61(02) 47360 085**

Abstract

Understanding the transportation and deposition (TD) of inhaled aerosol particles in human lung airways is important for health risk assessment and therapeutic efficiency of targeted drug delivery. The particle TD into a human lung depends on lung anatomy,-breathing pattern, as well as particle properties. The breathing capacity and lung airway diameters can be reduced by about 10% every 10 years after the age of 50. However, the age-specific particle TD in human lungs, particularly in the aged, has not been well understood in literature. This study investigates the particle TD in the lungs of people aged 50-70 years, using computational fluid dynamics (CFD). A new cutting method that splits the lung model into different sections has been developed as a feasible CFD method to simulate the particle TD in G0 to G14 lung airways. The inhalation of micron scale particles with three diameters (5 μm, 10 μm and 20 μm) and a constant air flow rate in inhalation is considered. It is found that different sized particles are deposited in different generation airways. Nearly 100% of 20 μm particles are deposited in the upper lung airways (G0-G5) and no particles pass through G7. Particles can go into deeper airways as their diameter decreases. When the particle size is decreased to 5 μm, over 48% of particles can pass through G14 and enter the deeper lung airways. An increase in age causes more particles to deposit in the upper airway and fewer particles to enter the deeper airways.

Keywords: Aging effect, Airflow, Aerosol particle transport and deposition (TD), Lung, Inhalation, Drug delivery, Cutting method.

1. Introduction:

Aerosol particle inhalation is commonly used as a drug delivery method to treat human lung diseases [1, 2]. Hence, the study of particle transportation and deposition (TD) in human lung airways is important, to ensure the effectiveness of drugs delivered through aerosol particle inhalation [3-5]. It is also important for reducing the effects of inhaled pollutant in the air on human health [6, 7].

Particle TD into non-realistic tracheobronchial lung airways has been studied extensively to analyse the airflow dynamics and particle TD in lung airways [8, 9]. Comer, et al. [10] developed a double bifurcation lung geometry based on Weibel's model [11], simulated airflow and TD in G3-G5 of this model numerically, and made a comprehensive comparison of their results with other numerical studies. Kleinstreuer et al. (2008) investigated airflow characteristics and particle TD of microparticles in a symmetric, triple bifurcation model of generations G0-G3. The results showed that the microparticles are mostly deposited at the carinal angles due to their strong inertial impaction mechanism. Zhang, et al. [12] studied the micro- and nano-size particle TD in a non-realistic, triple bifurcation model of generations G0-G3 using the Low-Reynolds-number (LRN) k–ω model. The nanoparticles were found to be more uniformly deposited in the airways than microparticles. Moreover, Islam, et al. [13] simulated aerosol particle transport in lung models using Large Eddy Simulations (LES) for up to 17 generations. The study shows that the majority of particles are deposited in the upper airways through an inertial impaction mechanism. However, they only discussed the total deposition efficiency of particles of all the 17 generations but not the deposition efficiency of each individual generation. Ahookhosh, et al. [14] conducted a detailed analysis of the evolution of various views of respiratory airway modelling throughout the years. This review study is helpful in understanding the limitations of lung anatomy and drug distribution in the lungs. CFD has proved to

be an efficient and accurate method for predicting the local particles deposition efficiency in the lung airways [15-20]. Deposition efficiency is defined as the percentage of aerosol particles absorbed in the human lung airways.

Some research on particle TD in realistic lung models has been conducted but mainly for small number of generations. Pourmehran, et al. [21] conducted CFD simulations of a realistic lung model of generations G0 to G6. The microparticles were found to be mostly deposited in the upper tracheobronchial lung airways. Recently, Asgari, et al. [22] studied the aerosol particles deposition in a realistic lung model of generations mouth to six (G6) based on the temperature and humidity conditions. The results showed that at very short timescales, aerosol evolution occurs mostly in the upper airway segments.

The earliest lung geometries created for simulating airflow in human lungs are mainly for adults [23]. The aerosol particle TD varies with age significantly, especially during the childhood/teenage stage and shrinks in older age. Xu and Yu [24] conducted a theoretical calculation of the PD of aerosol particles with diameters in the range between 0.01μm and 10 μm in the respiratory tracts of ages ranging from newborn babies to adults. It was found that the deposition efficiency in the mouth-throat section of children is higher than the adults. However, in the pulmonary and alveolar section, the opposite results were found [25]. Patterson, et al. [26]) studied nanoparticle deposition in the respiratory tract of school-aged subjects (8- to 18-year-olds). The results proved that the total particle deposition efficiency in the pulmonary section of children is higher than that of older people. The airborne particles deposit more easily for the school-aged people than adults because their lungs are smaller in size [27, 28]. Moreover, Deng, et al. [29] studied the age-specific (7-month old infant, 4-year old child and 20-year old adult) particle deposition in generation G3-G6 and G9-G12 lung airways through CFD simulations. The results further proved that the deposition efficiency of microparticles for children is higher than for adults in the tracheobronchial section. Compared to those conducted for younger people, few studies have investigated the airflow dynamics and particle TD in lung models

for the aged. The lung volume and breathing capacity of old people reduce with increased age [30]. Kim, et al. [31] analysed the airflow dynamics in the lungs of aged people and found that the pressure drop in the lung airways of 80-year-olds decreases by 38% compared to 50-year-olds. However, they did not study the particle TD in the lungs of aged people.

Because most people suffering from lung diseases are older, and the drug was usually prescribed for older people, it is important to improve the understanding of particle TD in their lungs. In addition, most studies of airflow and particle TD in the lungs considered a limited number (three or four) of generations. Airflow and particle TD in a whole lung using CFD has never been studied, due to consuming and unaffordable computing time.

In this paper, we employed an efficient cutting method to enable the CFD simulations to simulate airflow and particle TD in generations G0 to G14. This study does not investigate generations after G14 because the airway flow rate is very low after G14, and as a result, the inertial impaction deposition mechanism does not work properly [32]. The cutting method divides generations G0 to G14 into five sections, and each section includes three generations. The continuity of the airflow mass and the particle numbers is ensured at the boundaries of these sections. The details of the cutting method will be presented in section 3. The aim of this study is to understand the effects of particle size and age on the airflow and TD of particles in micrometer scales in human lungs. We consider the same inhaled air flow rate for all the ages, but varying airway diameters with age.

2. Lung model

Three-dimensional (3D) lung models with symmetric and planner lung airways from generation G0 to G14 are constructed based on the geometry proposed by Xu and Yu [24]. We used simplified lung models because geometries of realistic lung models with all the generations from G0 to G14 are not available and simulating complicated G0-G14 generation realistic lung model requires unaffordable computational time. To understand fundamental mechanisms of particle TD in a lung

model with many generations with affordable time, we used an efficient cutting method and simplified lung model. The solution of the present study will provide good understanding how particle TD is affected by the particle size and age, though quantitatively have difference from the realistic lung. Many researchers have studied human lungs in people aged up to 30 years [25, 33]. The lung geometries for older people are not straightforwardly available but can be generated based on the conclusions made in previous studies. The lung airway diameters of adults change little between those aged 30 and 50 years [34]. Therefore, we have assumed that a 50-year-old lung is the same as a 30-year-old lung. The 3D bifurcation symmetric lung airways of a 50-year old of up to generation G14 are generated by SolidWorks using the geometric parameters given by Xu and Yu [24] and presented in Fig. 1. The triple-bifurcation lung geometries of 60-year and 70-year old lungs (G0-G3, G3-G6, G6-G9, G9-G12, G12-G15) are generated by reducing airway diameter of each generation by 10% after every 10-year age [30, 31]. Furthermore, the size of the alveolar sacs grows with age [35]. Because tissue parameter and lung morphology of the human lung have changed due to the ageing. Between the ages of 50 and 80, lung tissue becomes around 7% stiffer [36]. Lung compliance is a volumetric number that is dependent on lung size and represents the lung's elastic property. Compliance is described as the ability of the lung tissue to absorb the same applied force, which is usually caused by a change in pressure. In general, as people get older, they become more compliant[37]. Lung compliance is an extrinsic parameter that rises as the size of the alveolar sacs grows. Low-compliance lungs are stiff lungs that require a lot more pressure to obtain the same capacity. To affect the capacity of the lungs, a stiff lung would require a larger than typical shift in pleural pressure, making breathing more difficult. As a result, we looked at lung compliance in order to determine elastic characteristics as people age. The details of the geometric parameters of the lung airways are listed in Table 1.

Table 1 Geometric parameters of lung airways generated use the method by Xu and Yu [24]

Generation (G)	Diameter (cm)			Length (cm)
	50 year old	60 year old	70 year old	50-70 years
0	1.665	1.499	1.332	12.286
1	1.220	1.098	0.976	4.284
2	0.830	0.747	0.664	1.896
3	0.560	0.504	0.448	0.759
4	0.450	0.405	0.360	1.268
5	0.350	0.315	0.280	1.071
6	0.280	0.252	0.224	0.901
7	0.230	0.207	0.184	0.759
8	0.186	0.167	0.149	0.639
9	0.154	0.139	0.123	0.538
10	0.130	0.117	0.104	0.460
11	0.109	0.098	0.087	0.390
12	0.095	0.086	0.076	0.330
13	0.082	0.074	0.066	0.271
14	0.074	0.067	0.059	0.231
15	0.066	0.059	0.053	0.202

As shown in Fig. 1, generation G0 has one bifurcation and the number of bifurcations of the *n*-th generation is 2^n. Simulating the airflow of all the generations from G0 to G14 using CFD without any simplification would mean unaffordable computing time. To enable CFD to simulate airflow in all the generations in affordable time, we cut the lung model into five sections: G0-G3, G3-G6, G6-G9, G9-G12, G12-G15, and their geometries are shown in Fig. 1. The airflow and particle of each section is simulated separately, considering the continuity of air mass and particle mass at the interfaces between generations.

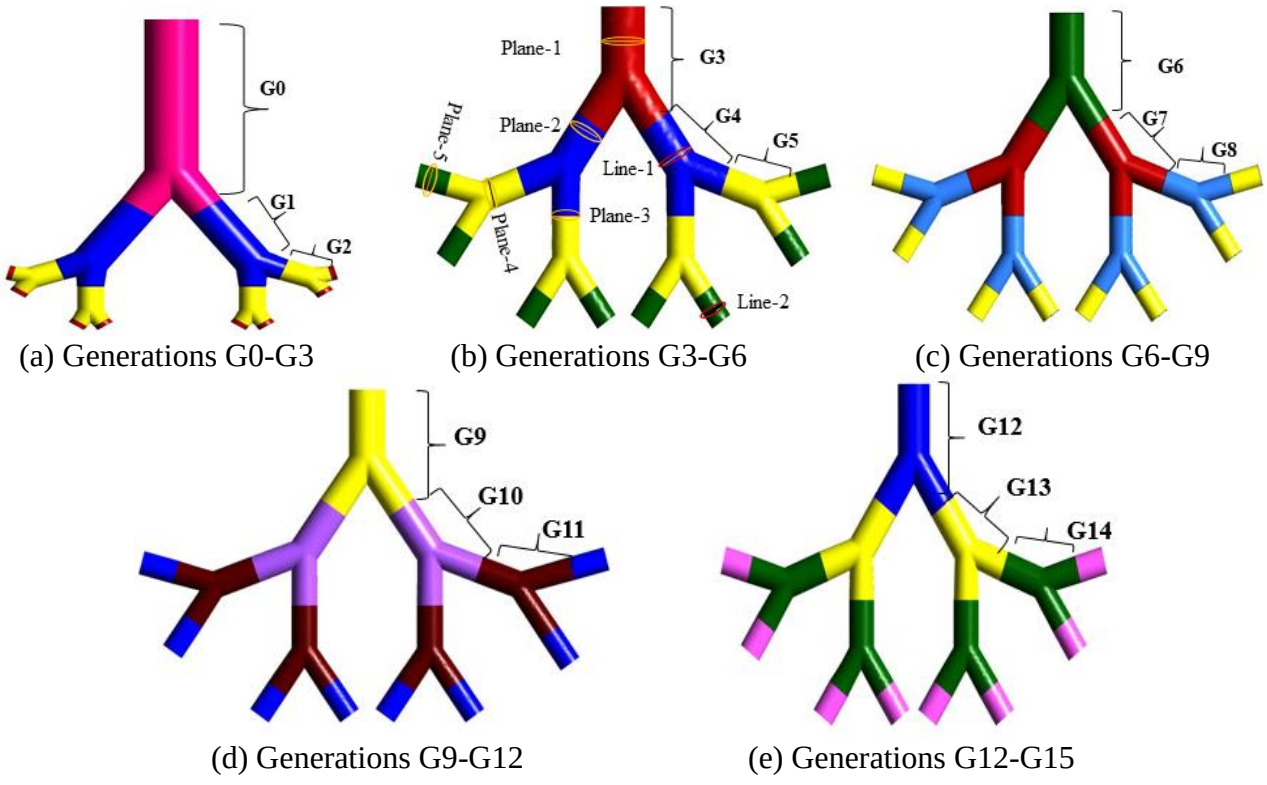

(a) Generations G0-G3 (b) Generations G3-G6 (c) Generations G6-G9

(d) Generations G9-G12 (e) Generations G12-G15

Fig. 1. Tracheobronchial triple bifurcation lung airways model (G0-G14) for the 50-year-old lung

3. **Numerical method**

3.1. Airflow model

The airflow in lung airways is solved using software ANSYS FLUENT. The governing equations for airflow are the Reynolds-averaged Navier-Stokes (RANS) equations:

$$\frac{\partial \rho}{\partial t} + \frac{\partial}{\partial x_i}(\rho \vec{u}_i) = 0 \qquad (1)$$

$$\frac{\partial}{\partial t}(\rho\vec{u}_i) + \frac{\partial}{\partial x_j}(\rho\vec{u}_i\vec{u}_j) = -\frac{\partial p}{\partial x_i} + \frac{\partial}{\partial x_j}\left[\mu\left(\frac{\partial\vec{u}_i}{\partial x_j} + \frac{\partial\vec{u}_j}{\partial x_i}\right)\right] + \frac{\partial}{\partial x_j}(-\rho\overline{u_i'u_j'}) \quad (2)$$

where $\vec{u}$ is the fluid velocity, μ is the molecular viscosity, ρ is the fluid density, p is the air pressure. The term $\rho\overline{u_i'u_j'}$ is the Reynolds stresses related to the turbulence model. The turbulence is simulated by the realisable k-ε turbulence model, which was proved to perform better than the standard k-ε model in various flow conditions including: rotating homogeneous shear flows; boundary-free shear flows; channel and flat boundary layer flows with and without pressure gradients; and backward facing step flows [38]. The realisable k-ε model was proved to be able to accurately predict the mean flow rate of complex lung geometries [39-42].

The second-order upwind and the pressure-velocity coupling scheme are used to solve the RANS equations. The velocity inlet and the pressure outlet boundary conditions have been given in the triple bifurcation symmetric lung airway model. In the simulation of each section in Fig. 1, the velocity at the inlet boundary is given and zero gauged pressure condition is considered at the exits [43-45]. The effects of unsteady inhalation profile in unsteady flow on particle TD were studied in some studies [46, 47]. However, a constant velocity is given at the inlet boundary of each section instead of an unsteady inhalation profile in order to testify the effectiveness of the current cutting method without the influence of the velocity variation. The airway wall was considered stationary, and the wall surfaces of airways was treated as no-slip walls [48-50].

If the inhaled air flow rate is considered to be evenly distributed among all the 2^n bifurcations of generation G-n, the inlet air flow rate of each bifurcation of G-n is $Q_e^n = Q/2^n$, where Q is the inlet flow rate at G0. Therefore, the inlet velocity of each section starting from G-n is calculated by:

$$u = Q_e^n/A_n \quad (3)$$

where A_n is the cross-sectional area of the inlet.

3.2. Particle transport and deposition model

The current model is a one-way coupling model that consider the particle transportation in air flow without considering the effect of the particles on the airflow. When the volume concentration of the particles is greater than 15%, two-way models that considers particle–particle interaction are required. However, the volume concentration is much less than 15% in all the drug delivery applications [51]. To simulate transportation of dilute, suspended particles in the human lung, collision-free condition can be implemented, or particle–particle interaction can be ignored [52]. Most of the published literature did not consider particle-particle interaction because direct particle-particle interactions can be ignored if the particle suspension entering the tracheobronchial airway is dilute [51]. In this paper, the interaction of the continuous and discrete phases has been accomplished by the Discrete Phase Model (DPM) model.

The Lagrangian approach is applied to determine the particle TD in human lung airways. The force balance equation of each individual particle is represented as:

$$\frac{d\vec{u}_p}{dt} = F_D\left(\vec{u} - \vec{u}_p\right) + \frac{\vec{g}}{\rho_p}\left(\rho_p - \rho\right) \quad (4)$$

where $\vec{u}$ and $\vec{u}_p$ are the fluid and particle velocities, respectively, $\vec{g}$ is the gravitational acceleration, ρ_P is the particle density, which is 1100 kg/m^3 [53, 54]. $F_D\left(\vec{u} - \vec{u}_p\right)$ is the drag force per unit particle mass, and the coefficient F_D is calculated by:

$$F_D = \frac{18\mu}{\rho_p d_p^2} C_D \frac{Re_P}{24} \quad (5)$$

where C_D is the drag coefficient calculated by [55] :

$$C_D = a_1 + \frac{a_2}{Re_P} + \frac{a_3}{Re_P{}^2} \quad (6)$$

The particle Reynolds number (Re_P) is defined as:

$$Re_P = \rho d_P \left|\vec{u}_p - \vec{u}\right| / \mu. \quad (7)$$

and a_1, a_2, a_3 are functions of the Reynolds number Re_P given by:

$$a_1, a_2, a_3 = \begin{cases} 0, & 24, & 0 & 0 < R_e < 0.1 \\ 3.690, & 22.73, & 0.0903 & 0.1 < R_e < 1 \\ 1.222, & 29.17, & 3.89 & 1 < R_e < 10 \\ 0.617, & 46.50, & -116.67 & 10 < R_e < 100 \\ 0.364, & 98.33, & -2778 & 100 < R_e < 1000 \\ 0.357, & 148.62, & -47500 & 1000 < R_e < 5000 \\ 0.46, & -490.546, & 578700 & 5000 < R_e < 10000 \\ 0.519, & -1662.5, & 5416700 & R_e > 10000 \end{cases}$$

The maximum Reynolds numbers based on the airway diameter at G0 are 5480, 6052 and 6855 for 50-,60- and 70-year ages, respectively. For particle deposition purposes, a trap condition is considered on the lung airways wall and an escape condition is considered at all outlets [56, 57]. Specifically, if a particle collides with the inner wall of an airway, it will be trapped by the wall surface (i.e. the coefficient of restitution is zero).

3.3 Deposition Efficiency calculation

The local deposition efficiency of the *n*-th generation is defined as the percentages of the particles absorbed (trapped) in this generation of airways out of the particles released at the inlet boundary of each section, and it is represented by $\eta_{L,n}$, where the subscript n stands for *n*-th generation. In the simulations, 79800 spherical particles with a uniform diameter were injected randomly from the inlet surface at one time at the inlet of each section. The deposited particle numbers are then converted by the local deposition efficiency using Eq. (8).

$$\eta_{L,n} = \frac{\text{Number of particles are trapped in a lung airways}}{\text{Total number of particles released at the inlet of this section}} \quad (8)$$

In a lung, G0-G14 are divided into five sections, and the number of particles at the inlet boundary of each section is smaller than the previous section because of the absorption of particles in the previous section. As a result, the global deposition efficiency (η_n) of the *n*-th section is calculated by:

$$\eta_n = \eta_{L,n} \times (1 - \sum_{i=1}^{K} \eta_i) \quad (9)$$

where K stands for the number of generations in all the previous sections. The percentage of particles that escape from all the outlets of each generation and enter the deeper lung is defined as particle escaping rate. The formula for calculating the particle escaping rate of generation n (α_n) is:

$$\alpha_n = 1 - \sum_{i=1}^{n} \eta_i \quad (10)$$

3.4. Grid dependency study and model validation

3.4.1. Grid dependency test

The grid dependency test is performed by conducting numerical simulations of G3-G6 at $d_p = 10\ \mu m$ using six meshes with the same mesh structure but different mesh densities. The smallest grid sizes next to the wall of Mesh 1 and Mesh 6 are 0.8 mm and 0.235 mm, respectively. The node numbers of Meshes 1 to 6 range from 172726 to 865461. Fig. 2 (b) shows the mesh near one bifurcation of generation G4. Ten-layers of smooth inflation are implemented near the wall to accurately predict the wall boundary flow inside the lung airway, as seen in Fig. 2 (a). The mesh structure of all other generations is similar to that shown in Fig. 2.

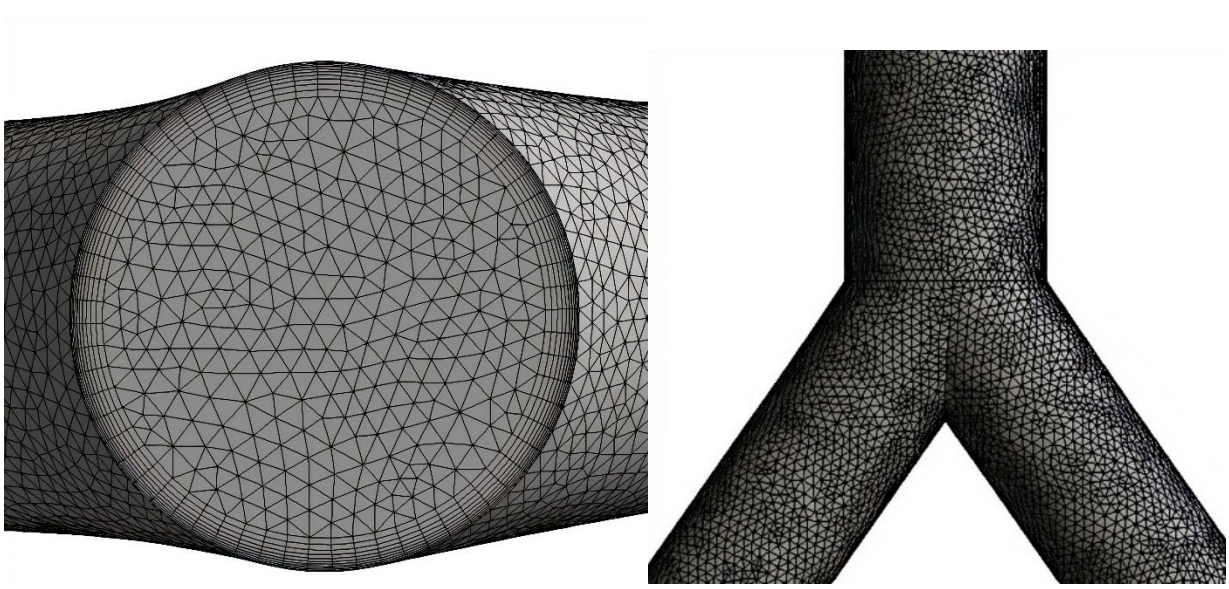

Fig. 2. Computational mesh for the section of G4 (a) Refined inflation mesh near the airway wall (b) The mesh resolution on the airway wall.

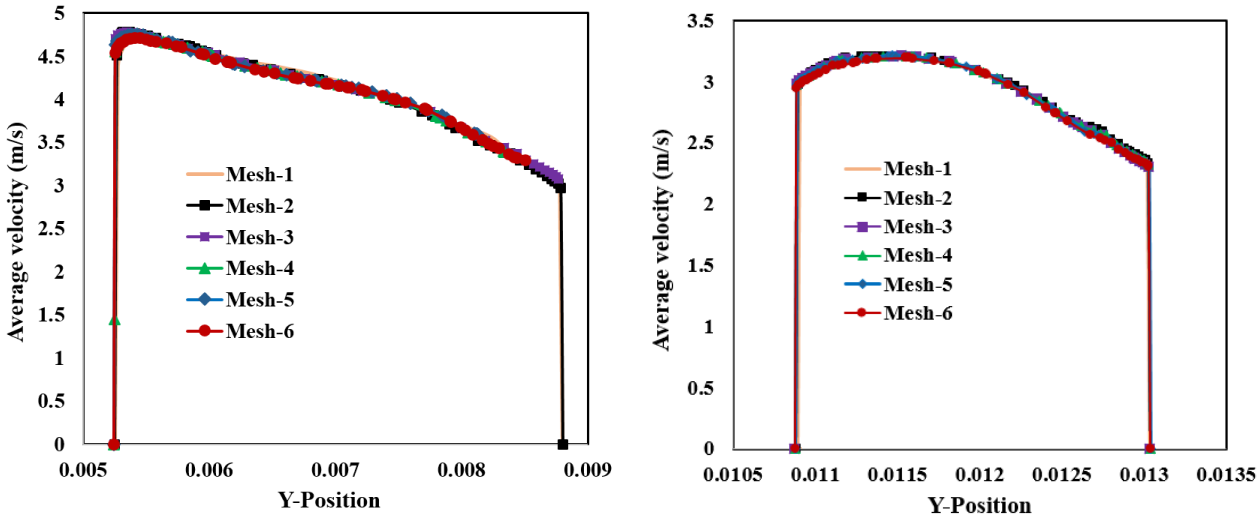

Fig. 3. Velocity distributions along the two lines indicated in Fig. (b) from six meshes for G3-G6 model, 50-year of age, particle diameter of $d_p = 10\ \mu m$ and inlet flow rate of 60 l/min. (a) Line-1 (b) Line-2.

The velocity distributions along two lines indicated in Fig. 1 (b) calculated from the six meshes are shown in Fig. 3. The velocity distribution of all the meshes follow the same trend and very small differences can be observed between different meshes. Particularly, the maximum velocity difference between Mesh 5 and Mesh 6 is 0.0174%.

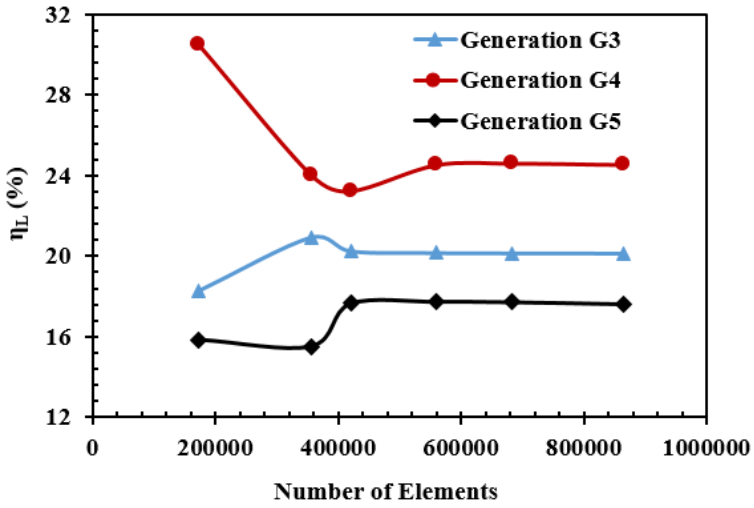

Fig. 4. Comparison of local deposition efficiency as functions of the grid number for G3-G6 of the 50-year age model, particle diameter of $d_p = 10\ \mu m$ and inlet flow rate of 60 l/min.

The variations of the local deposition efficiency with the element numbers of the mesh are presented in Fig. 4. The local deposition efficiencies nearly remain unchanged as the mesh density is higher than Mesh-4 with about 0.56 million elements. In the rest of the paper, we used the density of Mesh-5 with 0.68 million elements to do all the numerical simulations.

3.4.2 Model validation

The present CFD method is validated against available published data of airflow and particle TD in G3-G5 at Re=1000 and 2000 [58-60]. The inhalation flow rates 3.87 $l/\min$ ($Re = 1000$) and 7.78 $l/\min$ ($Re = 2000$)are calculated based on the inlet diameter of G3. Simulations are conducted for particle diameters of dp=1μm, 3μm, 5μm, 6μm, 7μm, 8μm and 10μm. Fig. 5 (a) and (b) shows the comparison of the total deposition efficiency of G3 and G4 against the Stokes number, respectively. The Stokes number is defined as:

$$\mathrm{St} = \frac{\rho_p d_p^2 u}{18\mu D}$$

where D represents the hydraulic diameter, which is the same as the inlet diameter of G3; u is the flow velocity at the inlet of G3. The one-way and two-way coupling models result in similar results in Fig. 5, because the concentration of particles in the air in drug delivery is so small that the airflow is not affected by the particle motion. It can be found that the deposition efficiency increases with the increase of the Stokes number. The variation trend of the deposition efficiency with the Stokes number is in good agreement with other numerical results and the experimental data, demonstrating that the present model is accurate to calculate the particle TD in the tracheobronchial airways of a lung. In Fig. 5, the deposition efficiencies of Re=1000 and 2000 do not differ from each other, indicating the deposition efficiency is mainly controlled by St.

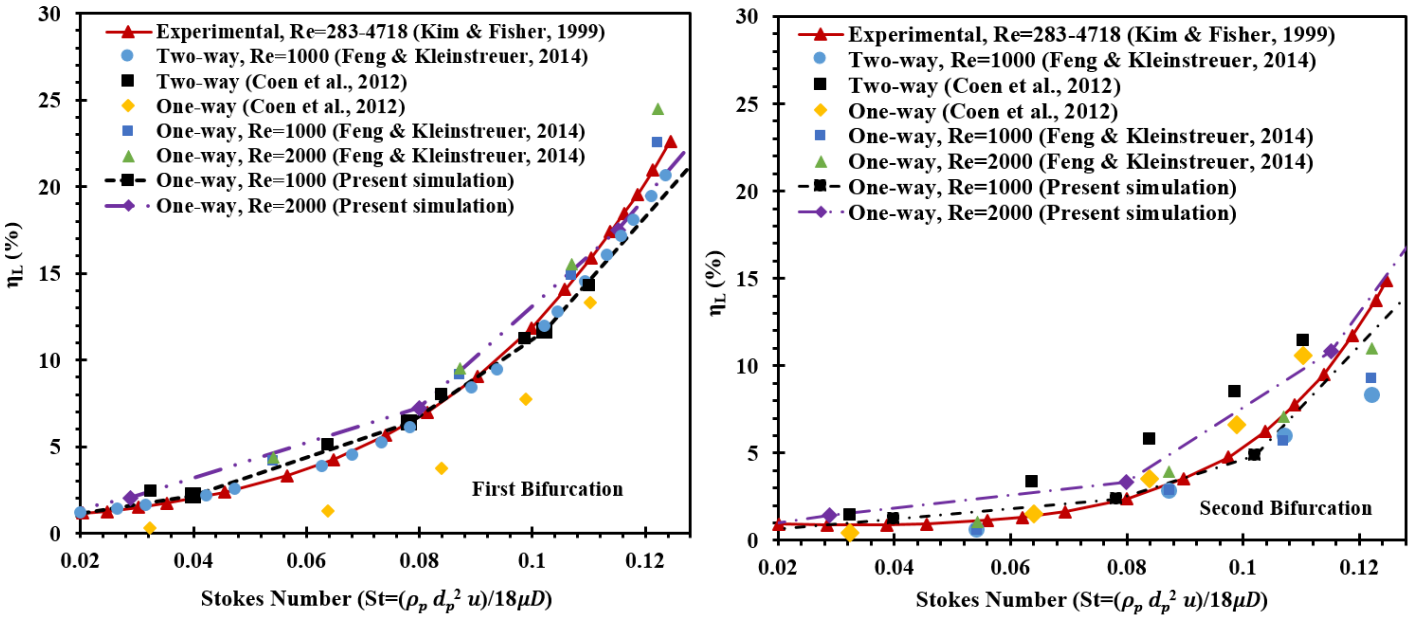

Fig. 5: Comparison between present simulation results of deposition efficiency of G3-G5 and results from literature [58-60]: (a) Generation G3; (b) Generation G4.

4. Results and discussion

In the present study, the inhalation flow airflow rate of $Q = 60$ l/min at G0 [61, 62] is considered for different ages and the inlet velocities of the five sections and three ages are listed in Table 2. However, the inhalation velocity profile affects the calculation of particle deposition in human lung airways. Kadota, et al. [46] studied the constant and inhalation flow pattern *to calculate* particles deposition in a realistic human airway. The results showed that vortex generation employing an inhalation flow pattern aided particle deposition in the airways. Ahookhosh, et al. [47] investigated an experimental for particles deposition in a realistic lung model of generations mouth to four (G4) considering three constant flow rates. The results showed that the deposition density increased with an increased flow rate. The inhalation route (mouth and nasal) has influence particle deposition in upper and tracheobronchial lung airways [63]. However, the results showed that the inhaling route had no effect on the distribution of deposited particles downstream of the trachea.

Hence, the inlet velocity changes with changes in the lung geometry for different ages of people. Aging has been associated with progressive decline in lung function and depends on the breathing parameters such as tidal volume and breathing frequency. The breathing frequency for 50-year, 60-year, and 70-year are 13.65(min^{-1}), 13.19(min^{-1}), and 12.92 (min^{-1}) respectively. Moreover, the tidal volumes are 500 ml, 403 ml and 179 ml for 50-year, 60-year, and 70-year respectively [34].

Table 2. Inlet airflow velocities for the five sets of models

Generations	50-Years	60-Years	70-Years
G0-G3	4.591	5.667	7.173
G3-G6	5.079	6.271	7.937
G6-G9	2.536	3.131	3.963
G9-G12	1.048	1.295	1.639
G12-G15	0.344	0.425	0.538

4.1. Airflow Characteristics

The air density and viscosity are 1.225 kg/m^3 and 1.79×10^{-5} kg/m·s respectively. Simulations are conducted for three particle diameters of d_p=5 μm, 10 μm and 20 μm and three ages in Table 2. Fig. 6 shows the airflow velocity contours on the symmetric plane within the lung generations G3-G6 of the three ages. The variation of velocity inside other sections are qualitatively similar to that of section G3-G6. The velocity decreases as air goes into the deep lung because the total cross-sectional area increases. For a constant flow rate, the 70-year-old lung model in Fig. 6 has the maximum velocity because it has the smallest lung diameter. The velocity varies significantly in each bifurcation area in the lung airways. After the air passes through the splitting point of each bifurcation, the velocity increases locally as the result of the streamline contraction. The local increase of the velocity and the sudden change of the velocity direction at the bifurcation point enhances the potential of particle deposition due to impaction mechanism.

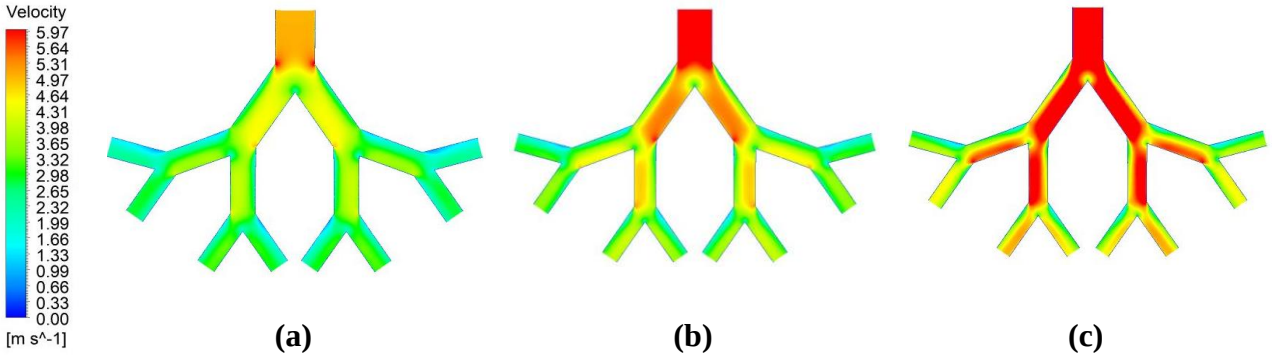

Fig. 6. Airflow velocity contours for generation G3-G6 at a flow rate of 60 l/min. (a) 50-years-old (b) 60-years-old, and (c) 70-years-old model.

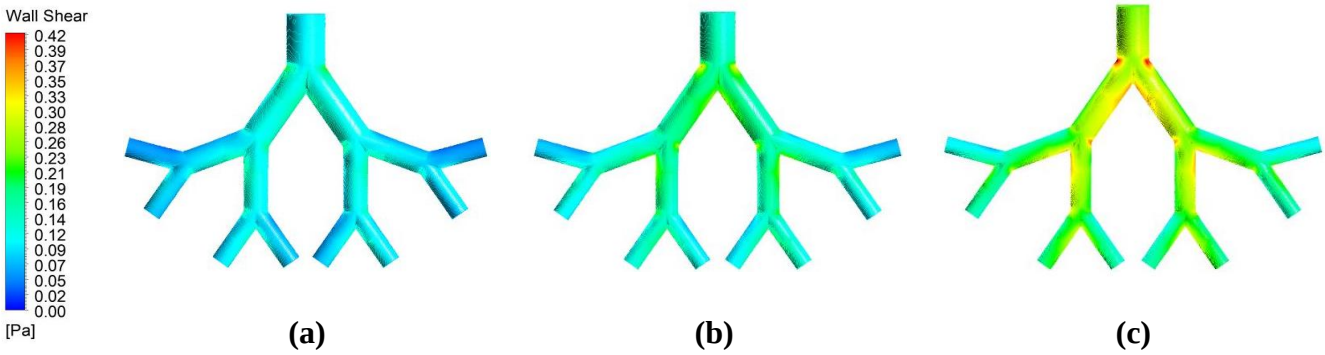

Fig. 7. Wall shear stress for generations G3-G6. (a) 50-years-old (b) 60-years-old, and (c) 70-years-old models.

Fig. 7 shows the distributions of airflow-induced wall shear stress along the inner wall of G3-G6 lung airways for the three ages. The localised velocity increase at the splitting point of each generation shown in Fig. 6 leads to the local increase in the wall shear. The motion of the fluid and particles near the wall can be understood by observing the wall shear stress, which is proportional to the velocity in the boundary layer flow next to the wall. The wall shear stress changes significantly in each lung airway generation because the flow resistance happens at complex lung geometry. At each sharp edge, the wall

shear stress is increased significantly because of the flow contraction. The maximum wall shear stress occurs in the splitting point of each bifurcation. Fig. 8 quantitatively shows the maximum area-weighted average wall shear stress on five sectional planes indicated in Fig. 1(b). With a contact inhaled air flow rate, the wall shear stress increases with the increase in age, as shown in Fig. 8.

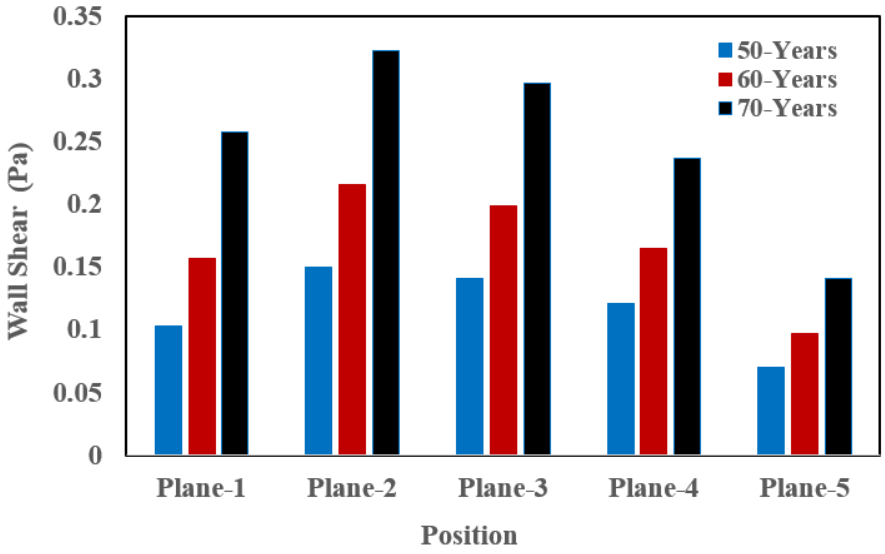

Fig. 8: Area-weighted average wall shear stress at different planes of the three ages' lung models for generation G3-G6 at a flow rate of 60 $l/\min$; see Fig. 1(b) for plane numbers.

The maximum area-weighted average static pressures at different positions in the section G3-G6 lung airways are shown in Fig. 9. The maximum pressure is observed at plane-1 (Fig.-1b) for all ages. In addition to the decrease in velocity as shown in Fig. 6, the pressure also decreases gradually when the airflow goes into the deep lung. The flow energy reduces as the airflow goes into deep lung because of the friction from the inner wall of the airways. The high velocity at 70-year-old lung shown in Fig. 6 requires high pressure at the inlet to drive the flow. Fig. 9 shows a 72.38% pressure increase for 70-year-old people compared to the 50-year-old in the lung airways. Therefore, breathing air into the lung for a 70-year-old is more complicated than for a 50-year-old. A significant pressure at Plane 5 is

decreased compared with that at plane 1, mainly because of the volume flow rate decrease. Hence, the decrease in velocity led to the low pressure drop in plane 5.

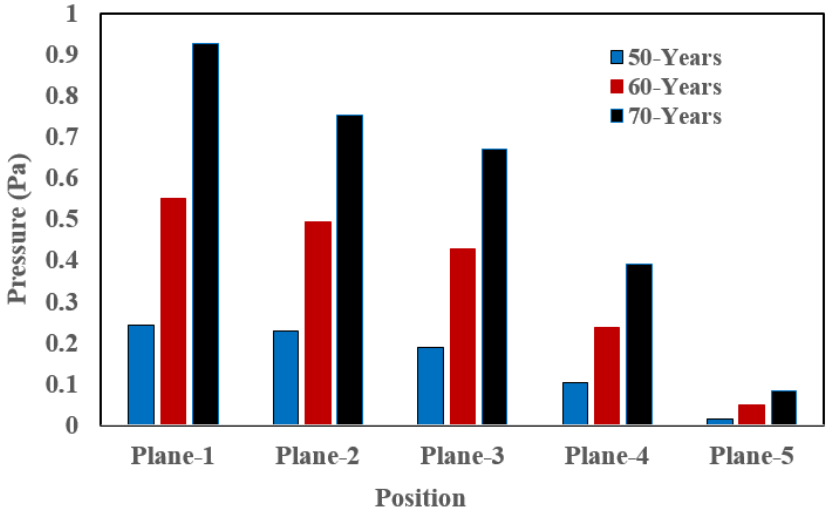

Fig. 9: Pressure at different planes of 50-70-year-old ages' model for generations G3-G6 at a flow rate of 60 $l/\min$; see Fig. 1(b) for plane numbers.

4.2 Particle Deposition

Fig. 10 shows the visualisation of local particle distribution of different sized particles at generation G3-G6 of 50-year age. The calculated local total particle deposition efficiencies of G3-G6 are 90.83%, 62.93% and 10.45% for of 20 µm, of 10 µm and 5 µm particles, respectively. The 5-µm particles have much smaller deposition efficiency than 20 µm particles at Generation G3-G6, because the impaction mechanism becomes weak as particle diameter decreases. Moreover, the 5-µm particles are more evenly distributed in each bifurcation lung area compared to the larger particles. When particle size is small, the inertia mechanism becomes weak. When the flow direction changes, small particles can change direction and follow the flow easily and as a result, they can spread, and deposition occurs at different areas. When the particle size is large, the inertia effect makes particles hit the wall at the first and second bifurcations. Even if the flow direction bends, large particles change their

direction slowly and do not follow the flow direction easily. This reduces the chance of large particle deposition in other places.

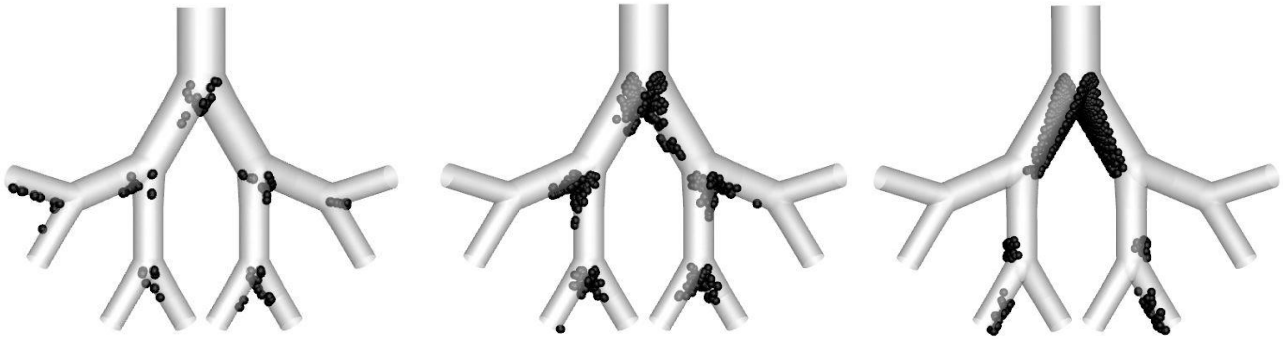

(a) d_s=5 µm (b) d_s=10 µm (c) d_s=20 µm

Fig. 10. Local Particle Deposition for the 50 years age for generation G3-G6 (a) 5 µm particles, (b) 10 µm particles, and (c) 20 µm particles at flow rate of 60 l/min

Fig. 11 shows the effects of the age on the global particle deposition efficiency in lung airway generations G0-G14. When the particle size is 5 µm, more particles can go deeper into the lung and the deposition efficiency in upper lung airways reduces significantly, compared with 10 µm and 20 µm. Around 0.61%, 0.28% and 0.11% of 5 µm particles are deposited at the generation G14 for 70-years, 60-years and 50-years of age, respectively (Fig. 11a). The maximum deposition efficiency of 10 µm particles is found at generation G4, G2 and G2 for the 50-, 60- and 70-year ages, respectively. With a constant inhaled flow rate, the decrease in the diameter of the G0 lung airway (as the result of aging) causes an increase in the velocity and higher Stokes number. It has been reported that the higher Stokes number causes higher deposition efficiency in the upper generations, as shown in Fig. 5. As the age increases, the increase of the flow velocity causes large deposition efficiency at early generations. In a younger age, the deposition efficiencies of early generations are small, allowing more

particles to pass upper generations and deposit in the deeper lung. Unlike 20 μm particles that are all trapped before G8, very small amount of 10 μm particles (0.09% for a 50-year-old) can reach G14.

The position of the maximum deposition efficiency is found to move towards the deep lung as the particle diameter decreases. The maximum deposition rate of 20 μm particles occurs at G0 and the majority of the 20 μm particles are deposited in the upper lung airways up to G4 because of the strong impaction mechanism at large particles. No 20 μm particles can pass through G8, resulting in zero deposition efficiency in all the generations after G8, as shown in Fig. 11 (c). More 20 μm particles are deposited at G0 than all other generations for all the three ages in Fig. 11 (c). The deposition efficiency of 20 μm particles in G0 for 70-years, 60-years, and 50-years of age people, are 50.83%, 38.62%, and 29.69%, respectively. The deposition efficiency increases in upper generations and decreases in lower generations with the increase in age. All the 20 μm particles are deposited between G0 to G8 generations for those of 50-70 years old, leaving no deposition after G9 (Fig. 11c). The deposition efficiency in the deeper lung airways for a 5 μm particle is better than 10 μm and 20 μm. Hence, the results suggest that the capacity for particle absorption in the deep lung airway generation (G14) for 50-year-olds is better than 70-year-olds.

The escaping rate from generations G0-G14 for 50-, 60- and 70-year ages are represented in Fig. 12. The escape rate at G14 are the percentage of particles that can pass G14 and enter generations after G15. The effects of the age and particle size on the escaping rate is opposite to their effects on the deposition rate. An increase in the deposition rate makes the escaping rate decrease with the increase in age (Fig. 12a). The escaping rates at G14 of 20-μm particles are zero for all the ages. Only 0.64%, 0.09% of 20-μm particles pass G6 and go into the deeper lung for 50-years, 60-years age lung models, respectively. The 20-μm particles cannot pass G5 of a 70-years age lung because all particles are deposited in the upper lung airways.

The escaping rates of 5-μm particles at every generation is significantly increased compared with 20-μm. Percentages of 66.65%, 53.51%, and 39.59% of 5-μm particles can pass G14 and go into the

deeper lung airways for 50-year, 60-year, and 70-year-olds, respectively (Fig. 12(a)). The escaping rates of 10-μm particles at G14 of all the three ages are not zero but much smaller than those of 5-μm particles (Fig. 12b); 3.12% of 10-μm particles pass G14 and enter G15 for the 50-year age, while only 0.12% of particles can enter G15 for the 70-year age.

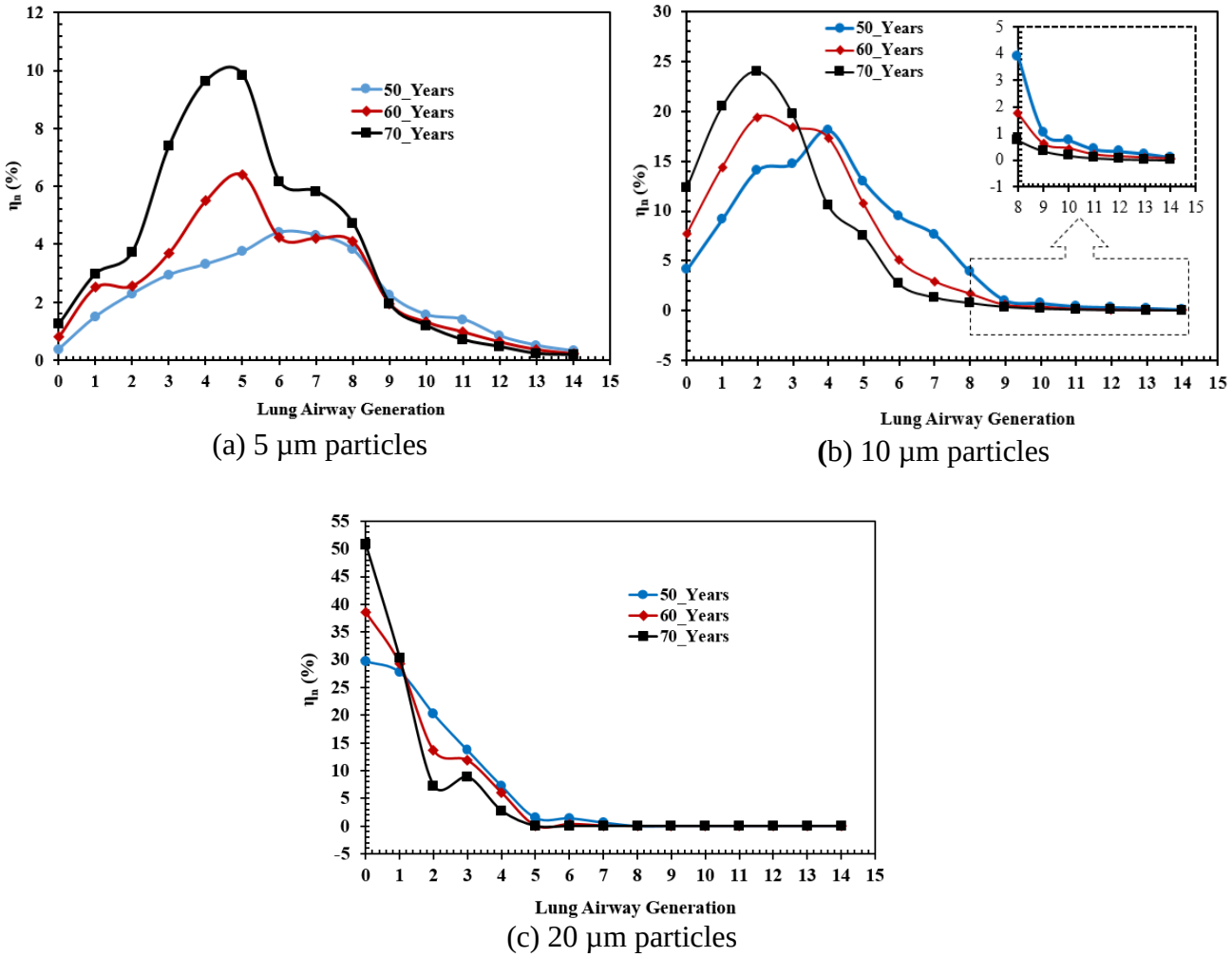

(a) 5 μm particles

(b) 10 μm particles

(c) 20 μm particles

Fig. 11. Effects of age on the global particle deposition efficiency in airway lung generation G0-G14 for: (a) 5 μm particles, (b) 10 μm particles, and (c) 20 μm particles

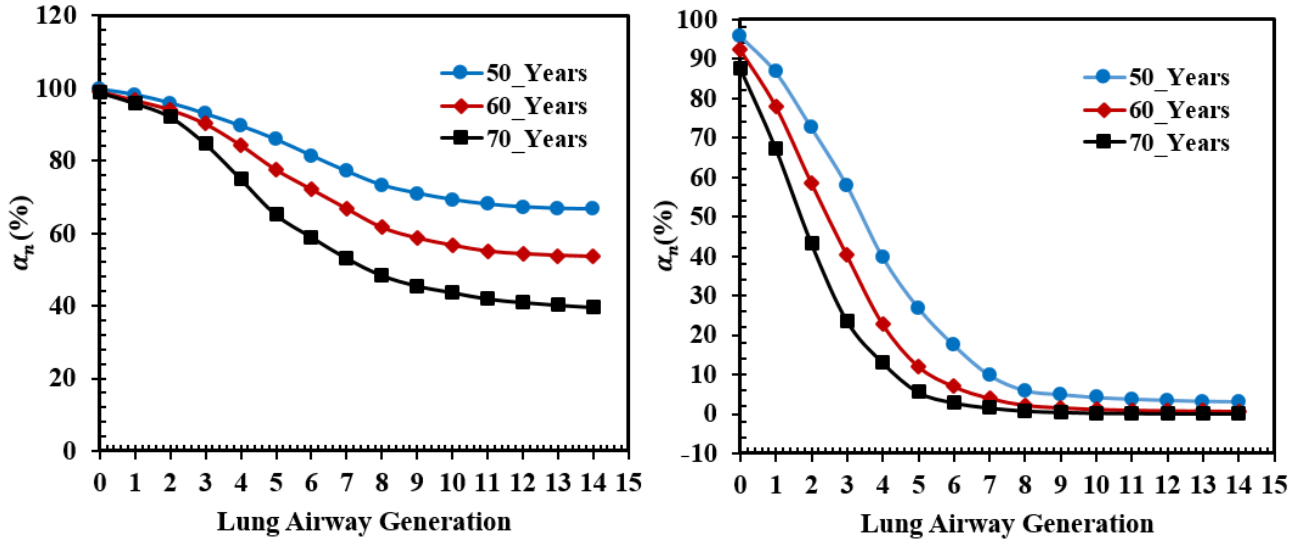

(a) 5 µm particles

(b) 10 µm particles

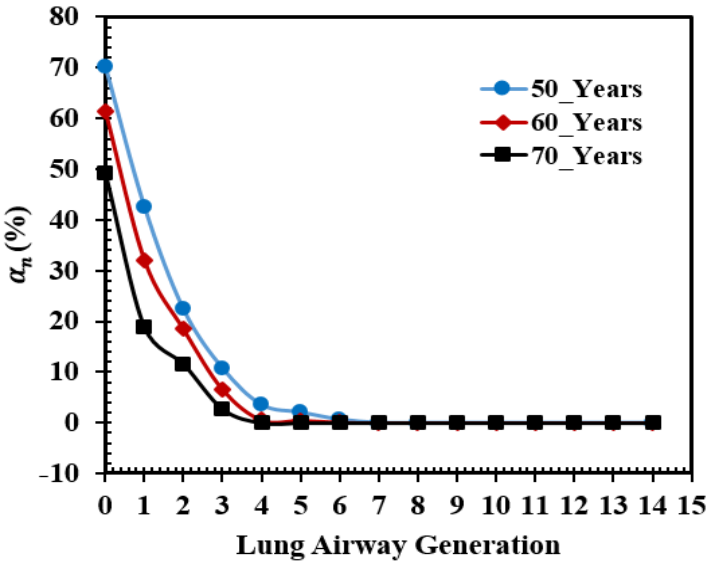

(c) 20 µm particles

Fig. 12 Particle escaping through rate (α_n) for ages 50-70 years at a flow rate of 60 l/min: (a) 5 µm particles, (b) 10 µm particles, and (c) 20 µm particles

5. Conclusions

The microparticles TD in the Tracheobronchial lung airway generations G0-G14 for 50-, 60- and 70-year-old lung models are investigated numerically. We have developed a cutting method to enable the airflow and particle TD in generations from G0 to G14 of a lung to be simulated using

computational fluid dynamics. The effects of age and particle diameter on the airflow and particle TD are discussed in detail and the conclusions are summarised as follows.

- The airflow velocity in the airways increased with increase of age due to the reduction of airway diameters. The local increase in wall shear stress is observed in each bifurcation lung airway because the flow resistance happens in that area. If the gauged pressure is zero at the exit at G15, the pressure in the lung airways increases with the increase of age. The pressure of G3 to G6 of a 70-year-old lung is 27.62% higher than that of a 50-year-old lung.
- Different sized particles are deposited in different positions of the lung. For a 50-year-old lung, 5-μm, 10-μm and 20-μm particles are mostly deposited in G6, G5 and G0, respectively. However, as the age increases to that of a 70-year-old, the maximum deposition rates of 5-μm, 10-μm and 20-μm particles occur at G5, G2 and G0, respectively.
- When the particle size is 20 μm, a high percentage of the particles (over 85%) are deposited in the upper lung airways (G0-G4). As the particle size is decreased to 5 μm, 52% of the particles are deposited in the lung airways, allowing over 48% of particles to enter the deep lung after G14. The above finding indicates that particles must have a small diameter to treat diseases in the deep lung.
- The numerical study showed that deposition efficiency is affected by ages. Most of the particles are deposited in 70-year-olds rather than 50-year-olds in the upper generations. The capacity for the particles to escape each generation decreases with the increase of age. The results suggest that to increase the number of particles deposited into deep lung airways, the particle size needs to be reduced. Therefore, our results indicate that the particles as targeted drug delivery should be provided based on the appropriate age [64, 65].

There are some limitations in this study that should be addressed in future studies. First, only an inhalation condition was considered in the simulation of particle TD. We will consider the inhalation as well as the exhalation process for both deposition and clearance of particles in the forthcoming studies. Second, we considered the micron-size ($5\mu m \leq d_p \leq 20$ μm) particle deposition in the G0-G14.

The PD of nanoparticle in airways is mainly governed by the Brownian diffusion mechanism. We will investigate nanoscale particles in future studies. Third, we considered symmetric and planner lung airways, instead of real lungs due to unavailability of the lung geometry. Nonetheless, the symmetric and planner lung airways model can predict the particle deposition pattern correctly [66, 67]. Even considering the above limitations, the airflow characteristic and particle deposition pattern in our present study are valid, based on the published literature.

Conflicts of Interest

The authors state no conflict of interest.

Acknowledgement

The authors would like to acknowledge the computing facility at WSU.

REFERENCES

[1] A. Kuzmov, T. Minko, Nanotechnology approaches for inhalation treatment of lung diseases, Journal of controlled release, 219 (2015) 500-518.

[2] G. Pulivendala, S. Bale, C. Godugu, Inhalation of sustained release microparticles for the targeted treatment of respiratory diseases, Drug delivery and translational research, 10 (2020) 339-353.

[3] L. Gradon, T.R. Sosnowski, Formation of particles for dry powder inhalers, Advanced Powder Technology, 25 (2014) 43-55.

[4] M. Paul, R. Lau, Potentials and challenges of Levodopa particle formulation for treatment of Parkinson's disease through intranasal and pulmonary delivery, Advanced Powder Technology, 31 (2020) 2357-2365.

[5] K. Ikegami, Y. Kawashima, H. Takeuchi, H. Yamamoto, D.-I. Momose, N. Saito, N. Isshiki, In vitro inhalation behavior of spherically agglomerated steroid particles with carrier lactose, Advanced Powder Technology, 11 (2000) 323-332.

[6] C.I. Davidson, R.F. Phalen, P.A. Solomon, Airborne particulate matter and human health: a review, Aerosol Science and Technology, 39 (2005) 737-749.

[7] R. Nieder, D.K. Benbi, F.X. Reichl, Soil-Borne Gases and Their Influence on Environment and Human Health, in: Soil Components and Human Health, Springer, 2018, pp. 179-221.

[8] M.S. Islam, S.C. Saha, T. Gemci, I.A. Yang, E. Sauret, Z. Ristovski, Y. Gu, Euler-Lagrange prediction of diesel-exhaust polydisperse particle transport and deposition in lung: anatomy and turbulence effects, Scientific Reports, 9 (2019) 1-16.

[9] Z. Li, C. Kleinstreuer, Z. Zhang, Particle deposition in the human tracheobronchial airways due to transient inspiratory flow patterns, Journal of aerosol science, 38 (2007) 625-644.

[10] J. Comer, C. Kleinstreuer, S. Hyun, C. Kim, Aerosol transport and deposition in sequentially bifurcating airways, J. Biomech. Eng., 122 (1999) 152-158.

[11] E.R. Weibel, Geometric and dimensional airway models of conductive, transitory and respiratory zones of the human lung, in: Morphometry of the human lung, Springer, 1963, pp. 136-142.

[12] Z. Zhang, C. Kleinstreuer, J.F. Donohue, C. Kim, Comparison of micro-and nano-size particle depositions in a human upper airway model, Journal of aerosol science, 36 (2005) 211-233.
[13] M.S. Islam, S.C. Saha, E. Sauret, T. Gemci, Y. Gu, Pulmonary aerosol transport and deposition analysis in upper 17 generations of the human respiratory tract, Journal of Aerosol Science, 108 (2017) 29-43.
[14] K. Ahookhosh, O. Pourmehran, H. Aminfar, M. Mohammadpourfard, M.M. Sarafraz, H. Hamishehkar, Development of human respiratory airway models: A review, European Journal of Pharmaceutical Sciences, 145 (2020) 105233.
[15] C. Kleinstreuer, Z. Zhang, J. Donohue, Targeted drug-aerosol delivery in the human respiratory system, Annu. Rev. Biomed. Eng., 10 (2008) 195-220.
[16] C. Ou, H. Jian, Q. Deng, Particle Deposition in Human Lung Airways: Effects of Airflow, Particle Size, and Mechanisms, Aerosol and Air Quality Research, 20 (2020).
[17] Z. Zhang, C. Kleinstreuer, C.S. Kim, Comparison of analytical and CFD models with regard to micron particle deposition in a human 16-generation tracheobronchial airway model, Journal of Aerosol Science, 40 (2009) 16-28.
[18] K. Kadota, T.R. Sosnowski, S. Tobita, I. Tachibana, J.Y. Tse, H. Uchiyama, Y. Tozuka, A particle technology approach toward designing dry-powder inhaler formulations for personalized medicine in respiratory diseases, Advanced Powder Technology, 31 (2020) 219-226.
[19] S. Khorasanizade, M. Shams, B. Mansoori, Calculation of aerosol deposition in human lung airways using Horsfield geometric model, Advanced Powder Technology, 22 (2011) 695-705.
[20] T. Myojo, A. Ogami, T. Oyabu, Y. Morimoto, M. Hirohashi, M. Murakami, K. Nishi, C. Kadoya, I. Tanaka, Risk assessment of airborne fine particles and nanoparticles, Advanced Powder Technology, 21 (2010) 507-512.
[21] O. Pourmehran, T.B. Gorji, M. Gorji-Bandpy, Magnetic drug targeting through a realistic model of human tracheobronchial airways using computational fluid and particle dynamics, Biomechanics and Modeling in Mechanobiology, 15 (2016) 1355-1374.
[22] M. Asgari, F. Lucci, A.K. Kuczaj, Multispecies aerosol evolution and deposition in a human respiratory tract cast model, Journal of Aerosol Science, 153 (2021) 105720.
[23] H. Landahl, On the removal of air-borne droplets by the human respiratory tract: I. The lung, The bulletin of mathematical biophysics, 12 (1950) 43-56.
[24] G. Xu, C. Yu, Effects of age on deposition of inhaled aerosols in the human lung, Aerosol Science and Technology, 5 (1986) 349-357.
[25] B. Asgharian, M. Menache, F. Miller, Modeling age-related particle deposition in humans, Journal of aerosol medicine, 17 (2004) 213-224.
[26] R.F. Patterson, Q. Zhang, M. Zheng, Y. Zhu, Particle deposition in respiratory tracts of school-aged children, Aerosol Air Qual. Res, 14 (2014) 64-73.
[27] F. Hruba, E. Fabianova, K. Koppova, J.J. Vandenberg, Childhood respiratory symptoms, hospital admissions, and long-term exposure to airborne particulate matter, Journal of Exposure Science & Environmental Epidemiology, 11 (2001) 33-40.
[28] W. Roemer, G. Hoek, B. Brunekreef, J. Clench-Aas, B. Forsberg, J. Pekkanen, A. Schutz, PM10 elemental composition and acute respiratory health effects in European children (PEACE project). Pollution Effects on Asthmatic Children in Europe, European Respiratory Journal, 15 (2000) 553-559.
[29] Q. Deng, C. Ou, J. Chen, Y. Xiang, Particle deposition in tracheobronchial airways of an infant, child and adult, Science of the Total Environment, 612 (2018) 339-346.
[30] D.E. Niewoehner, J. Kleinerman, Morphologic basis of pulmonary resistance in the human lung and effects of aging, Journal of applied physiology, 36 (1974) 412-418.
[31] J. Kim, R.L. Heise, A.M. Reynolds, R.M. Pidaparti, Aging effects on airflow dynamics and lung function in human bronchioles, PloS one, 12 (2017).
[32] P. Koullapis, S.C. Kassinos, M.P. Bivolarova, A.K. Melikov, Particle deposition in a realistic geometry of the human conducting airways: Effects of inlet velocity profile, inhalation flowrate and electrostatic charge, Journal of biomechanics, 49 (2016) 2201-2212.

[33] J. Xi, A. Berlinski, Y. Zhou, B. Greenberg, X. Ou, Breathing resistance and ultrafine particle deposition in nasal–laryngeal airways of a newborn, an infant, a child, and an adult, Annals of biomedical engineering, 40 (2012) 2579-2595.
[34] W. Hofmann, Mathematical model for the postnatal growth of the human lung, Respiration physiology, 49 (1982) 115-129.
[35] J.M. Turner, J. Mead, M.E. Wohl, Elasticity of human lungs in relation to age, Journal of applied physiology, 25 (1968) 664-671.
[36] S.J. Lai-Fook, R.E. Hyatt, Effects of age on elastic moduli of human lungs, Journal of applied physiology, 89 (2000) 163-168.
[37] W. Wahba, Influence of aging on lung function-clinical significance of changes from age twenty, Anesthesia & Analgesia, 62 (1983) 764-776.
[38] T.H. Shih, W.W. Liou, A. Shabbir, Z. Yang, J. Zhu, A new k-ϵ eddy viscosity model for high reynolds number turbulent flows, Computers and Fluids, 24 (1995) 227-238.
[39] V.K. Srivastav, A.R. Paul, A. Jain, Capturing the wall turbulence in CFD simulation of human respiratory tract, Mathematics and Computers in Simulation, 160 (2019) 23-38.
[40] C. Ball, M. Uddin, A. Pollard, High resolution turbulence modelling of airflow in an idealised human extra-thoracic airway, Computers & Fluids, 37 (2008) 943-964.
[41] Z. Tian, J. Tu, G. Yeoh, CFD studies of indoor airflow and contaminant particle transportation, Particulate Science and Technology, 25 (2007) 555-570.
[42] N.M. Isa, A.N.K. Ahmad Fara, N.Z. Asmuin, Investigation on the Turbulence Models Effect of a Coal Classifier by Using Computational Fluids Dynamics, in: Applied Mechanics and Materials, Trans Tech Publ, 2014, pp. 617-621.
[43] H. Luo, Y. Liu, Modeling the bifurcating flow in a CT-scanned human lung airway, Journal of Biomechanics, 41 (2008) 2681-2688.
[44] R.K. Freitas, W. Schröder, Numerical investigation of the three-dimensional flow in a human lung model, Journal of Biomechanics, 41 (2008) 2446-2457.
[45] M.S. Islam, G. Paul, H.X. Ong, P.M. Young, Y. Gu, S.C. Saha, A review of respiratory anatomical development, air flow characterization and particle deposition, International Journal of Environmental Research and Public Health, 17 (2020) 380.
[46] K. Kadota, N. Inoue, Y. Matsunaga, T. Takemiya, K. Kubo, H. Imano, H. Uchiyama, Y. Tozuka, Numerical simulations of particle behaviour in a realistic human airway model with varying inhalation patterns, Journal of Pharmacy and Pharmacology, 72 (2020) 17-28.
[47] K. Ahookhosh, S. Yaqoubi, M. Mohammadpourfard, H. Hamishehkar, H. Aminfar, Experimental investigation of aerosol deposition through a realistic respiratory airway replica: an evaluation for MDI and DPI performance, International journal of pharmaceutics, 566 (2019) 157-172.
[48] A. Farghadan, K. Poorbahrami, S. Jalal, J.M. Oakes, F. Coletti, A. Arzani, Particle transport and deposition correlation with near-wall flow characteristic under inspiratory airflow in lung airways, Computers in Biology and Medicine, (2020) 103703.
[49] M. Rahimi-Gorji, T.B. Gorji, M. Gorji-Bandpy, Details of regional particle deposition and airflow structures in a realistic model of human tracheobronchial airways: two-phase flow simulation, Computers in biology and medicine, 74 (2016) 1-17.
[50] M.M. Rahman, M. Zhao, M.S. Islam, K. Dong, S.C. Saha, Airflow dynamic and particle deposition in age-specific human lungs, Australasian Fluid Mechanics Conference, Brisbane, QLD, (2020).
[51] M.S. Islam, S.C. Saha, E. Sauret, H. Ong, P. Young, Y. Gu, Euler–Lagrange approach to investigate respiratory anatomical shape effects on aerosol particle transport and deposition, Toxicology Research and Application, 3 (2019) 2397847319894675.
[52] Y. Tsuji, Multi-scale modeling of dense phase gas–particle flow, Chemical engineering science, 62 (2007) 3410-3418.
[53] M.S. Islam, Y. Gu, A. Farkas, G. Paul, S.C. Saha, Helium–Oxygen Mixture Model for Particle Transport in CT-Based Upper Airways, International Journal of Environmental Research and Public Health, 17 (2020) 3574.

[54] A. Moskal, T.R. Sosnowski, Dynamics of aerosol pulse in a simplified mouth-throat geometry and its significance for inhalation drug delivery, Chemical Engineering and Processing, 30 (2009) 545-558.
[55] S. Morsi, A. Alexander, An investigation of particle trajectories in two-phase flow systems, Journal of Fluid mechanics, 55 (1972) 193-208.
[56] M.S. Islam, S.C. Saha, T. Gemci, I.A. Yang, E. Sauret, Y. Gu, Polydisperse microparticle transport and deposition to the terminal bronchioles in a heterogeneous vasculature tree, Scientific reports, 8 (2018) 1-9.
[57] W. Zhang, Y. Xiang, C. Lu, C. Ou, Q. Deng, Numerical modeling of particle deposition in the conducting airways of asthmatic children, Medical engineering & physics, 76 (2020) 40-46.
[58] Y. Feng, C. Kleinstreuer, Micron-particle transport, interactions and deposition in triple lung-airway bifurcations using a novel modeling approach, Journal of Aerosol Science, 71 (2014) 1-15.
[59] X. Chen, W. Zhong, X. Zhou, B. Jin, B. Sun, CFD–DEM simulation of particle transport and deposition in pulmonary airway, Powder technology, 228 (2012) 309-318.
[60] C.S. Kim, D.M. Fisher, Deposition characteristics of aerosol particles in sequentially bifurcating airway models, Aerosol Science & Technology, 31 (1999) 198-220.
[61] C. Kleinstreuer, Z. Zhang, Laminar-to-turbulent fluid-particle flows in a human airway model, International Journal of Multiphase Flow, 29 (2003) 271-289.
[62] A.J. Hickey, T.B. Martonen, Y. Yang, Theoretical relationship of lung deposition to the fine particle fraction of inhalation aerosols, Pharmaceutica Acta Helvetiae, 71 (1996) 185-190.
[63] F. Lizal, J. Elcner, J. Jedelsky, M. Maly, M. Jicha, Á. Farkas, M. Belka, Z. Rehak, J. Adam, A. Brinek, The effect of oral and nasal breathing on the deposition of inhaled particles in upper and tracheobronchial airways, Journal of aerosol science, 150 (2020) 105649.
[64] S.P. Newman, Drug delivery to the lungs: challenges and opportunities, Therapeutic delivery, 8 (2017) 647-661.
[65] N. Labiris, M. Dolovich, Pulmonary drug delivery. Part I: physiological factors affecting therapeutic effectiveness of aerosolized medications, British journal of clinical pharmacology, 56 (2003) 588-599.
[66] Q. Deng, C. Ou, Y.-M. Shen, Y. Xiang, Y. Miao, Y. Li, Health effects of physical activity as predicted by particle deposition in the human respiratory tract, Science of The Total Environment, 657 (2019) 819-826.
[67] C. Kleinstreuer, Z. Zhang, Z. Li, Modeling airflow and particle transport/deposition in pulmonary airways, Respiratory physiology & neurobiology, 163 (2008) 128-138.